Journal of Molecular Structure 1118 (2016) 219–232

Contents lists available at ScienceDirect

Journal of Molecular Structure

journal homepage: http://www.elsevier.com/locate/molstruc

Spectroscopic (FT-IR, FT-Raman, UV, ^{1}H and ^{13}C NMR) profiling and theoretical calculations of (2*E*)-2-[3-(1*H*-imidazol-1-yl)-1-phenylpropylidene]hydrazinecarboxamide: An anticonvulsant agent

Nadia G. Haress [a], Munusamy Govindarajan [b, c, **], Reem I. AL-Wabli [a], Maha S. Almutairi [a], Monirah A. Al-Alshaikh [d], Abdulaziz A. Al-Saadi [e], Mohamed I. Attia [a, f, *]

[a] Department of Pharmaceutical Chemistry, College of Pharmacy, King Saud University, P.O. Box 2457, Riyadh 11451, Saudi Arabia
[b] Department of Physics, BGCW, Puducherry, India
[c] Department of Physics, AGCW, Karaikal, Puducherry, India
[d] Department of Chemistry, College of Sciences, King Saud University, Riyadh 11451, Saudi Arabia
[e] Department of Chemistry, King Fahd University of Petroleum and Minerals, Dhahran 31261, Saudi Arabia
[f] Medicinal and Pharmaceutical Chemistry Department, Pharmaceutical and Drug Industries Research Division, National Research Centre (ID: 60014618), El Bohooth Street, Dokki, Giza 12622, Egypt

ARTICLE INFO

Article history:
Received 25 January 2016
Received in revised form
7 April 2016
Accepted 8 April 2016
Available online 11 April 2016

Keywords:
Imidazole
FT-IR
FT-Raman
HOMO-LUMO
DFT/B3LYP

ABSTRACT

Vibrational characteristics of the anticonvulsant agent, (2*E*)-2-[3-(1*H*-imidazol-1-yl)-1-phenylpropylidene]hydrazinecarboxamide ((2*E*)-IPHC) have been investigated. The computational data are obtained by adopting *ab initio* Hartree-Fock (HF) and DFT/B3LYP/6-31 + G(d,p) methods. The most stable conformer is identified by a potential energy scan. The optimized geometrical parameters indicated that the overall symmetry of the most stable conformer is C_S. Atoms in molecules (AIM) analysis is contained out and the chemical bondings between the atoms are as characterized. Mulliken atomic charges and simulated thermo-molecular (heat capacity and enthalpy) characteristics of the (2*E*)-IPHC molecule also have been analyzed. The magnitude of the molecular electrostatic potential (MEP) of oxygen, hydrogen, and nitrogen atoms as well as phenyl and imidazole rings in the title molecule were investigated along with their contribution to the biological activity. The energy gap between HOMO and LUMO orbitals has been found to be 5.1334 eV in the gaseous phase. Excitation energies, oscillator strength and wavelengths were computed by the time-dependent density function theory (TD-DFT) approach. Predicted wavenumbers have been assigned and they are consistent with the experimental values. The ^{1}H and ^{13}C nuclear magnetic resonance (NMR) chemical shifts of the (2*E*)-IPHC molecule were computed by the gauge independent atomic orbital (GIAO) method and were compared with the experimental results.

1. Introduction

Epilepsy is an idiopathic ubiquitous syndrome that has been recognized as a serious brain disorder afflicting more than 60 million people according to epidemiological studies [1]. Annually, about 0.25 million new individuals are added to this figure [2]. Epilepsy is characterized by a sudden onset of spontaneous convulsive and non-convulsive seizures and episodes of sensory, motor or autonomic phenomenon with or without a loss of consciousness [3,4]. In spite of the enormous therapeutic arsenal of several generations of antiepileptic drugs (AEDs), only 65–75% of epileptic patients achieve adequate control with the currently available AEDs [5,6].

Conventional antiepileptic agents (carbamazepine and phenytoin) and recent antiepileptic drugs (loreclezole, vigabatrin, remacemide, and gabapentin) are clinically useful for the management of different types of epilepsy. Nevertheless, many AEDs have serious side effects [7–9]. Accordingly, the continued search for safer and more effective AEDs is necessary.

(2*E*)-2-[3-(1*H*-Imidazol-1-yl)-1-phenylpropylidene]

* Corresponding author. Department of Pharmaceutical Chemistry, College of Pharmacy, King Saud University, P.O. Box 2457, Riyadh 11451, Saudi Arabia.
** Corresponding author. Department of Physics, BGCW, Puducherry, India.
E-mail address: msamabd@yahoo.com (M.I. Attia).

http://dx.doi.org/10.1016/j.molstruc.2016.04.026
0022-2860/

hydrazincarboxamide ((2*E*)-IPHC) displayed anticonvulsant activity with 50% seizure protection at a dose of 972 μmol/kg in a subcutaneous pentylenetetrazole (scPTZ) screen and showed no neurotoxicity [10]. Although a literature review indicated that some spectroscopic studies of certain imidazoles already have been documented [11–13], the molecular structure of this molecule has not previously been reported using computational methods. Accordingly, the present work deals with vibrational investigations as well as spectral (FT-IR, FT-Raman, UV, ^{1}H and ^{13}C NMR) characterization of the (2*E*)-IPHC molecule by adopting both *ab initio* Hartree-Fock (HF) and DFT/B3LYP/6-31 + G(d,p) computational methods. Atoms in molecules (AIM), molecular electrostatic potential (MEP), and HOMO-LUMO analysis were also computed for the (2*E*)-IPHC molecule. It is thought that molecular characterization of the (2*E*)-IPHC compound will support the development of improved anticonvulsant agents.

2. Experimental details

2.1. General

The Fourier transform infrared spectrum of (2*E*)-IPHC molecule was recorded on a Perkin Elmer RXL spectrometer (Waltham, Massachusetts, USA) in the region 4000–400 cm^{-1}, with sample in the KBr pellet method. The resolution of the spectrum is 2 cm^{-1}. The FT-Raman spectrum was measured in the range 3500–50 cm^{-1} using a Bruker RFS 100/S FT-Raman spectrophotometer (Ettlingen, Germany.) with a 1064 nm Nd:YAG laser source of 100 mW power (Göttingen, Germany).

2.2. Synthesis

3-(1*H*-Imidazol-1-yl)-1-phenylpropan-1-one (0.86 gm, 4.3 mmol) was added to a suspension containing anhydrous sodium acetate (0.35 gm, 4.3 mmol) and semicarbazide hydrochloride (0.32, 4.3 mmol) in absolute ethanol (40 mL). The reaction mixture was stirred at ambient temperature for 18 h, filtered and the filtrate was evaporated under vacuum. The residue was crystallized from ethanol to give 0.44 gm (40%) of the title molecule m.p. (412–414 K) as white crystals which were suitable for X-ray analysis. ^{1}H and ^{13}C NMR as well as the mass spectral data of the title compound **2** are consistent with the previously reported ones [10].

3. Quantum chemical calculations

The quantum chemical calculations have been performed with AM1, HF, and DFT (B3LYP) methods using the Gaussian 03 program [14]. The minimum energy and optimized structural parameters have been evaluated for the calculations of vibrational frequencies at different levels of theories and variety of basis sets by assuming C_S point group symmetry. At the optimized geometry for the title molecule no imaginary frequency modes were obtained, therefore a true minimum on the potential energy surface was found. As a result, the calculated frequencies, reduced masses, force constants, infrared intensities, Raman intensities, and depolarization ratios were obtained. In order to improve the calculated values, a spectral uniform scaling factor was used to offset the systematic errors caused by basis set incompleteness, neglect of electron correlation, and vibrational anharmonicity. Hence, the vibrational frequencies were scaled by 0.9608 for B3LYP/6-31 + G(d,p) [15]. After using the scaling factor, the deviation from the experimental values was less than 10 cm^{-1} with a few exceptions. The Gaussview program [16] has been employed to acquire visual animation and also for the verification of the normal modes assignment. The potential energy distributions (PEDs) were computed from quantum chemically calculated vibrational frequencies using the VEDA program [17].

The UV electronic absorption spectra are computed with time-dependent density functional theory (TD-DFT) at the B3LYP/6-31 + G(d,p) level. Molecular electrostatic potential (MEP) is used to investigate the binding and reactive centers of the title compound. The changes in the thermodynamic functions (heat capacity, entropy, and enthalpy) are investigated at different temperatures from that of the vibrational frequency calculations of the (2*E*)-IPHC molecule. The NMR chemical shifts are computed with the gauge including atomic orbital (GIAO) method using B3LYP/6-31 + G(d,p). The HOMO-LUMO energy gap in different solvents is computed and analyzed using the polarizable continuum model (PCM).

4. Results and discussion

4.1. Synthesis

The target molecule (2*E*)-IPHC (**2**) was synthesized as portrayed in Scheme 1 using the commercially available acetophenone as a starting material according to our previously reported procedure [10].

4.2. Potential energy scan

A potential energy scan is mainly used to describe the relationship between potential energy and molecular geometry. The conformational analysis was used through the potential surface scan in order to determine the most optimized geometry of the (2*E*)-IPHC molecule. The torsional barrier rotations are in reference to the C–N and C–C bonds. The first two potential energy scan curves were carried out with dihedral angles C17–C18–N4–N5 and C17–C18–C19–C22, the link between the phenyl ring with semicarbazide and imidazole moieties, respectively. The third scan was carried out with dihedral angle C19–C18–N4–N5, the link between the imidazole ring and the semicarbazide moiety. During the scan, all the geometrical parameters were simultaneously relaxed and were varied in steps of 30° from 0 to 360°. The curves of the potential energy as a function of the dihedral angle were presented in Fig. 1. Thirteen conformers were obtained in each scan. Conformational analysis revealed that the most stable conformer was obtained in the third scan at a torsion angle of 180° with a global minimum energy of 81.1997 kcal/mol (0.129361 hartrees). After optimization with the global minimum energy, the phenyl ring and semicarbazide moiety are in one plane and the imidazole ring is parallel to that plane. The energies of the conformers of the (2*E*)-IPHC molecule were calculated by AM1 theory and they are listed in Table 1. The standard deviations of the conformational energies were calculated as 1.3929, 13.4253, and 10.9250 kcal/mol in scans 1, 2, and 3, respectively.

4.3. Molecular geometry structure details

The optimized molecular structure of the (2*E*)-IPHC molecule with the labeling of its atoms is shown in Fig. 2. The selected bond distances and bond angles of XRD [18] and the computed optimized geometrical parameters (HF and B3LYP) are presented in Table 2. The title molecule is composed of phenylpropyl, imidazole, and semicarbazide moieties. All C–H distances in the phenyl and imidazole rings showed similar values of about 0.930 Å, except for the alkenes C–H bond lengths (0.970 Å). Among the C–H bond lengths, C19–H20 had the maximum observed value. The C–N experimental bond distances in the semicarbazide and imidazole moieties of the (2*E*)-IPHC molecule are very close to the values computed by HF and B3LYP methods. The average values of the C–N single bond length in the semicarbazide and imidazole moieties were calculated as 1.326 Å and 1.350 Å, respectively. The C31=

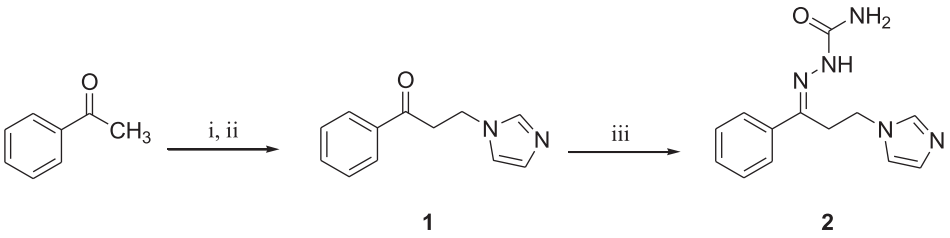

Reagents and conditions: (i) $HN(CH_3)_2{\cdot}HCl$, $(CH_2O)_n$, conc. HCl, ethanol, reflux, 2 h; (ii) imidazole, water, reflux, 5 h; (iii) semicarbazide hydrochloride, anhydrous sodium acetate, ethanol, RT, 18 hrs

Scheme 1. Preparation of the target compound **2**.

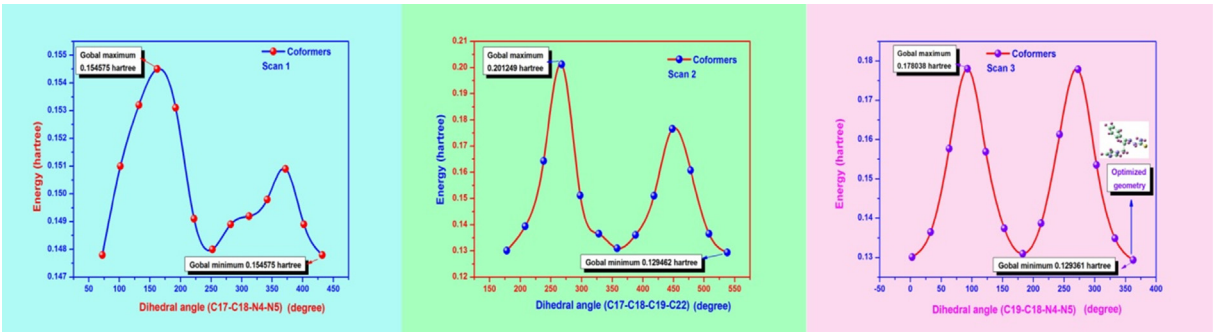

Fig. 1. Potential energy scan of (2*E*)-IPHC.

Table 1
Potential energy scan values of (2*E*)-IPHC.

Scan 1 C17–C18–N4–N5		Scan 2 C17–C18–C19–C22		Scan 3 C19–C18–N4–N5	
Initial dihedral angle	Energy (kcal/mol)	Initial dihedral angle	Energy (kcal/mol)	Initial dihedral angle	Energy (kcal/mol)
72	92.7459	178	81.6389	3	81.6389
102	94.7539	208	87.4748	33	85.5923
132	96.1344	238	103.0998	63	98.9582
162	96.9502	268	126.2549	93	111.696
192	96.0717	298	94.8794	123	98.4562
222	93.5616	328	85.6550	153	86.2198
252	92.8714	358	82.2037	183	82.2037
282	93.4361	388	85.4040	213	87.0355
312	93.6244	418	94.8166	243	101.2173
342	94.0009	448	110.8182	273	111.6339
372	94.6911	478	100.8408	303	96.3227
402	93.4361	508	85.7178	333	84.5882
432	92.7459	538	81.2624	363	81.1997

O1 and C18═N4 double bond were observed as 1.240 and 1.287 Å, respectively. The computed and observed C═N bond length is shorter than C–N. The hexagonal symmetry of the phenyl ring in the (2*E*)-IPHC molecule was distorted due to the differences in C–C bond values. The maximum increase of C–C bond length was observed as 1.392 Å. It is also justified by the values of 1.391 Å and 1.405 Å computed by the HF and B3LYP methods, respectively. The experimental N–N bond length was observed as 1.373 Å and its respective calculated value by both HF and B3LYP methods was 1.392 Å. Three N–H bond distances for N5–H32, N6–H33 and N6–N34 were observed in the semicarbazide moiety of the (2*E*)-IPHC molecule with the values of 0.829, 0.853 and 0.880 Å, respectively. The value of N6–34 was greater than the value of N6–N33 in the amide group, which might be due to the intramolecular attraction with the nearest oxygen atom.

The experimental bond angles in the phenyl ring showed an increase of bond angles C11–C9–C7 (120.9) and C15–C13–C11 (120.4), and a decrease of bond angle C13–C11–C9 (119.1) from 120°. Variation of the C–C–C torsion angles from 120° in the phenyl ring are another evidence of hexagonal symmetry distortion of the ring. The pulling effect of linking groups of the phenyl ring was shown by the decrease of the dihedral angle C13–C11–C9 value by 0.9° from 120°. The H–C–C torsion angles in the phenyl and imidazole rings were observed around 119° and 124°, respectively. Similarly, in the semicarbazide moiety the bond angles H34–N6–H33, O1–C31–N6, N5–N4–C18, and N6–C31–N5 appeared as 115°, 123°, 119°, and 117°, respectively.

4.4. Atoms in molecules (AIM) analysis

One of the most useful tools to characterize atomic and molecular interactions, particularly hydrogen bonding, is topological analysis using 'Atoms in molecules' (AIM) theory [19,20]. AIM theory is used to understand and guess the electron density and

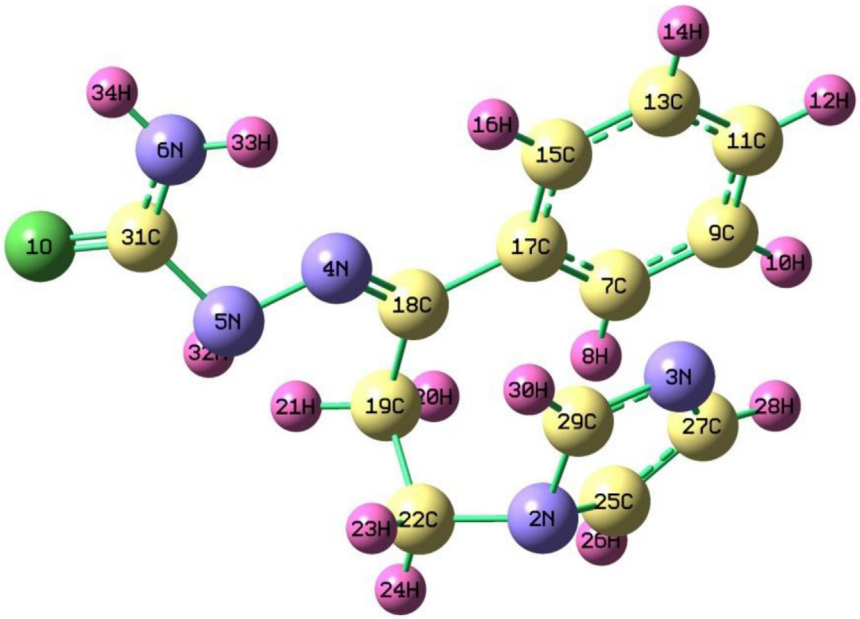

Fig. 2. Optimized geometric structures with atoms numbering of (2*E*)-IPHC.

Table 2
Selected optimized parameters of (*2E*)-IPHC.

Bond length	B3LYP	HF	Experimental [a]	Bond angle	B3LYP	HF	Experimental[a]
N5H32	1.017	0.996	0.829	H32N5N4	121.7	121.5	125.7
N6H33	1.010	0.991	0.853	H33N6C31	118.5	120.9	118.2
N6H34	1.008	0.991	0.853	H34N6H33	119.0	120.4	115.0
C7H8	1.087	1.076	0.930	H8C7C9	119.6	119.6	119.7
C9H10	1.086	1.075	0.930	H10C9C7	119.7	119.8	119.5
C11H12	1.086	1.075	0.930	H12C11C9	120.1	120.1	120.5
C13H14	1.086	1.075	0.930	H14C13C15	119.6	119.7	119.8
C15H16	1.087	1.076	0.930	H16C15C13	119.7	119.8	119.3
C25H26	1.080	1.069	0.930	H26C25C27	132.6	132.0	124.7
C27H28	1.082	1.070	0930	H28C27N3	121.3	121.6	124.7
C29H30	1.083	1.072	0930	H30C29N3	125.9	125.4	123.6
C19H20	1.098	1.086	0.970	H20C19C22	108.1	108.5	108.9
C19H21	1.094	1.083	0.970	H21C19H20	107.5	107.7	107.4
C22H23	1.094	1.083	0.970	H23C22N2	107.6	107.8	108.9
C22H24	1.095	1.084	0.970	H24C22H23	107.4	107.4	107.7
C31O1	1.222	1.201	1.240	O1C31N6	125.4	124.2	123.6
C18N4	1.291	1.260	1.287	N4C18C19	116.2	117.0	123.9
C29N4	1.315	1.290	1.366	C11C9C7	120.2	120.1	120.9
C27C25	1.373	1.351	1.349	C13C11C9	119.7	119.8	119.1
C9C7	1.394	1.384	1.380	C15C13C11	120.2	120.1	120.4
C11C9	1.396	1.386	1.375	C7C17C18	120.4	120.2	119.7
C13C11	1.396	1.385	1.369	N6C31N5	114.5	115.8	117.5
C15C13	1.395	1.385	1.383	C25C27N3	110.7	110.3	110.6
C7C17	1.405	1.391	1.392	C27N3C29	106.2	105.1	106.4
C29N2	1.369	1.350	1.371	C31N5N4	121.2	121.1	118.7
C31N6	1.367	1.349	1.332	N5N4C18	120.6	120.7	119.2
C27N3	1.377	1.369	1.313	C17C18C19	118.5	118.0	120.8
C31N5	1.401	1.376	1.369	C22N2C29	126.7	126.9	125.9
N4N5	1.357	1.352	1.373	C18C19C22	112.3	112.2	115.6
C17C18	1.495	1.447	1.486	C19C22N2	112.7	112.4	113.5
C22N2	1.456	1.501	1.460				
C18C19	1.513	1.512	1.509				
C19C22	1.543	1.533	1.529				

[a] Ref [18].

nature of the bond in complex molecules. According to AIM theory, any chemical bonding is characterized by the existence of a bond critical point (BCP). The BCPs have been located and various properties can be calculated at their coordinates in space. The AIM molecular graph showing the different bonds and ring critical points of the (2*E*)-IPHC are depicted in Fig. 3 and the topological parameters are given in Table 3.

The following parameters are based on the AIM theory as well as the Koch and Popelier criteria [21]: (i) the presence of BCP between the proton (H) and acceptor (Y) is a confirmation of the existence of a hydrogen bonding interaction; (ii) the value of the charge densities ρ_{BCP} of C—C and C—N bonds are computed within the range of

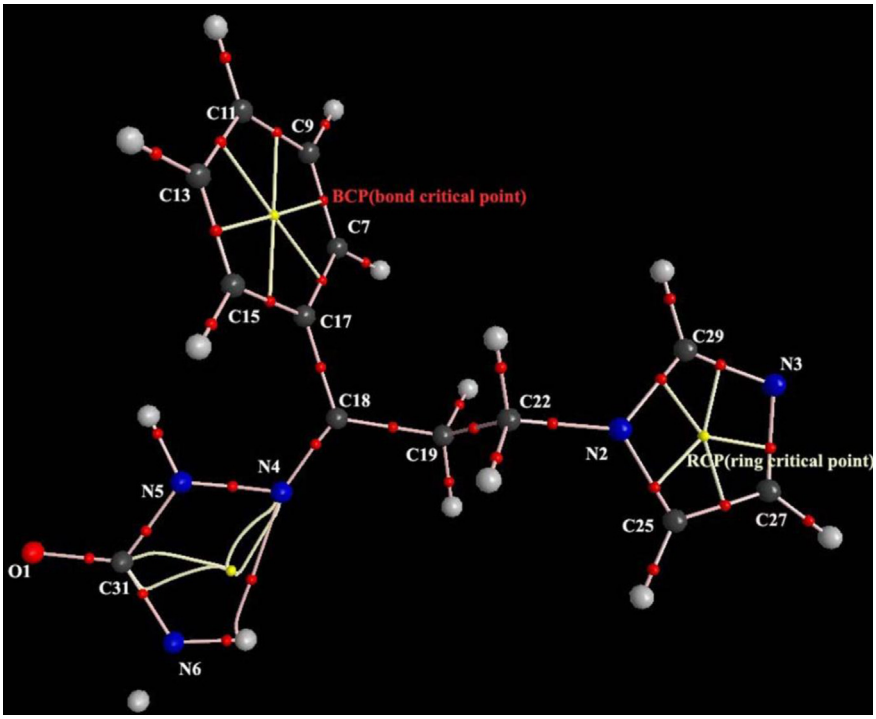

Fig. 3. AIM molecular graph of (2*E*)-IPHC.

Table 3
AIM analysis for the (*2E*)-IPHC molecule: electron density ρ_{BCP}, Laplacian of electron density $\Delta^2\rho_{BCP}$, electron kinetic energy density G_{BCP}, total electron energy density H_{BCP} and interaction energy E_{int} at bond critical points (BCPs).

BCP	ρ_{BCP} (a.u)	$\Delta^2\rho_{BCP}$ (a.u)	G_{BCP} (a.u)	H_{BCP} (a.u)	V_{BCP} (a.u)	E_{int} (kcal/mol)
C17–C15	0.2284	−0.8328	0.1008	−0.3090	0.4098	128.57
C15–C13	0.2954	−0.8712	0.1034	−0.3212	0.4246	133.21
C13–C11	0.2949	−0.8716	0.1024	−0.3204	0.4228	132.65
C11–C9	0.2946	−0.8700	0.1022	−0.3198	0.4220	132.40
C9–C7	0.2956	−0.8724	0.1035	−0.3216	0.4251	133.37
C7–C17	0.2900	−0.8400	0.1015	−0.3115	0.4130	129.57
C11–H12	0.2669	−0.7920	0.0434	−0.2413	0.2846	89.29
C17–C18	0.2471	−0.6488	0.0715	−0.2337	0.3052	95.75
C18–C19	0.2359	−0.5896	0.0676	−0.2150	0.2827	88.69
C19–C22	0.2213	−0.5244	0.0595	−0.1906	0.2501	78.46
N4–N5	0.2944	−0.4272	0.1545	−0.2613	0.4158	130.45
C31–N6	0.2972	−0.6068	0.1582	−0.3098	0.4680	146.83
C18–N4	0.3329	−0.5596	0.2890	−0.4289	0.7179	225.24
C22–N2	0.2261	−0.2852	0.1194	−0.1908	0.3102	97.32
C29–N2	0.2717	−0.3924	0.1860	−0.2741	0.4701	147.49
C29–N3	0.3276	−0.7228	0.1896	−0.3703	0.5600	175.70
C27–N3	0.2737	−0.4648	0.1418	−0.2580	0.3999	125.46
C25–N2	0.2625	−0.3520	0.1809	−0.2671	0.4501	141.21
C25–C27	0.3073	−0.8856	0.1208	−0.3422	0.4630	145.26
C31–O1	0.3700	−0.5744	0.3439	−0.4876	0.8315	260.88
N4···H33	0.0229	−0.0936	0.0228	−0.0006	0.0221	6.93
C27–H28	0.2707	−0.8120	0.0422	0.2454	0.2877	90.26
C22–H24	0.2654	−0.7828	0.0427	0.2383	0.2811	88.19

0.2213–0.2956 and 0.2261–0.3329 a.u. and the corresponding Laplacian $\nabla^2\rho_{BCP}$ at BCP should be within the range −0.8724 to −0.5244 a.u and −0.7228 to −0.2852 a.u. In addition, the electron density minimum (0.0229 a.u) and Laplacian $\nabla^2\rho_{BCP}$ maximum (−0.0936 a.u) values were calculated in N4···H33 intermolecular hydrogen bond. The terms G_{BCP}, H_{BCP}, and V_{BCP} describe the electron kinetic energy density, total electron energy density, and potential electron density, at BCP, respectively, while E_{int} describes the interaction energy at bond critical points. The highest E_{int} interaction energy was observed at the C═O bond as 260 kcal/mol. The lowest H_{BCP} was calculated as −0.4876 a.u. The decrease in H_{BCP} was observed with an increase of E_{int}.. Similarly, E_{int} was calculated for C18 = N4 as 225.24 kcal/mol and H_{BCP} as −0.4289 a.u. along the same trend.

4.5. Comparative Mulliken population analysis

Mulliken charge population of the (2*E*)-IPHC molecule was analyzed using the B3LYP method with regard to its compositional groups: phenylpropyl, imidazole and semicarbazide. The results are presented in Table 4. The horizontal bar diagram of comparative Mulliken atomic charges are shown in Fig. 4. The comparison

between the Mulliken charge distribution in the intact (2*E*)-IPHC molecule and its separated phenylpropyl moiety indicated that the Mulliken charge distribution is almost the same in the ring and the C17 is positive in both the (2*E*)-IPHC molecule and the phenylpropyl moiety; whereas the atoms C18 and C19 exhibited some deviation between the (2*E*)-IPHC molecule and the phenylpropyl moiety. This confirms an influence of the attachment of the imidazole ring in the (2*E*)-IPHC molecule. Similarly, the imidazole ring in the (2*E*)-IPHC molecule displayed deviation of Mulliken charges from that of the separated imidazole moiety in the atoms N2, N3, C25, and C27. The atomic charge of C25 in the (2*E*)-IPHC molecule is more positive as compared with that of the separated imidazole moiety. Mulliken charge at the N4 (−0.279821 e) atom is less negative than at the N5 (−0.4771 e) and N6 (−0.7571 e) atoms in the (2*E*)-IPHC molecule and they exhibited some deviation from those values at the separated semicarbazide moiety. Atom C31 (0.736084 e) in the (2*E*)-IPHC molecule was computed with the most positive charge due to its attachment to three electronegative atoms, namely two nitrogen atoms and one oxygen atom. All hydrogen atoms in the (2*E*)-IPHC molecule showed positive values and there was not much deviation in their charge distribution as compared with that in the compositional groups. Mulliken charges at the carbonyl and amide groups in the (2*E*)-IPHC molecule might contribute positively to its biological activity.

4.6. Molecular electrostatic potential (MEP)

A 3D plot of molecular electrostatic potential (MEP) is used as a visual method to analyze reactivity and relative polarity of atomic sites of molecules including biomolecules and drugs. The MEPs of (2*E*)-IPHC were computed at HF and B3LYP levels (Fig. 5) based on their optimized geometrical positions. The MEPs were computed to be between −0.06951 e and 0.06951 e in B3LYP and from −0.06166 e to 0.06166 e at the HF level.

The value of charges of MEP ranges from red (more negative) to blue (more positive). The negative ion sites were observed near an oxygen atom (O1) in the semicarbazide moiety and nitrogen atoms in the imidazole ring. Due to the electron withdrawing effect of O1, the nearby nitrogen atoms (N5 and N6) showed less negative potential. On the other hand, the positive ion sites were observed around the phenyl ring and methylene groups. The negative charge of the carbon atoms in the phenyl ring was diminished due to the effect of the other atoms attached to the phenyl ring. The magnitude of MEP of all hydrogen atoms was positive. Both positive and negative maxima were observed in the amide group, where the maximum positive value was located at H34 and the maximum negative potential was shown at N6.

Table 4
Comparative Mulliken charges of (*2E*)-IPHC and its compositional groups; phenylpropyl, semicarbazide and imidazole.

Atom	(*2E*)-IPHC	Phenylpropyl	Semicarbazide	Imidazole
O1	−0.520550		−0.535134	
N2	−0.365862			−0.611397
N3	−0.435363			−0.558599
N4	−0.279821		−0.590508	
N5	−0.477195		−0.456057	
N6	−0.757188		−0.729375	
C7	−0.168459	−0.175101		
H8	0.144444	0.123932		
C9	−0.131064	−0.137724		
H10	0.143965	0.126097		
C11	−0.122304	−0.129500		
H12	0.143447	0.124634		
C13	−0.128822	−0.129130		
H14	0.145912	0.126092		
C15	−0.183791	−0.181223		
H16	0.158293	0.121014		
C17	0.069557	0.160162		
C18	−0.215524	−0.321438		
C19	−0.317504	−0.293246		
H20	0.161568	0.153945		
H21	0.168236	0.142429		
C22	−0.163087	−0.312067		
H23	0.171220	0.154951		
H24	0.171646	0.144400		
C25	0.003864			−0.019444
H26	0.147826			0.136170
C27	−0.037504			0.035829
H28	0.133974			0.142275
C29	0.191298			0.115053
H30	0.149358			0.122198
C31	0.736084		0.666378	
H32	0.338202		0.345970	
H33	0.350224		0.313127	
H34	0.343871		0.364071	

4.7. Thermodynamic simulation properties of (2E)-IPHC

Some of the statistical thermodynamic functions like entropy (S), enthalpy changes (δH) and heat capacity (C_p) of (2E)-IPHC were simulated at the gas phase from the theoretical harmonic frequencies and the results are listed in Table 5. It can be observed that these thermodynamic functions increase with temperature over the range of 100–1000 K due to the fact that the molecular vibrational intensities increase with temperature [22]. The computed values of entropy and heat capacity attained the maximum and steady state was reached. The enthalpy change increases linearly at low temperatures and abruptly at high temperature. The correlation equations between entropy, enthalpy change, and heat capacity temperatures were fitted by quadratic formulas and the corresponding fitting factors (R^2) for these thermodynamic properties all have the same value of 0.9999. The corresponding fit equations are as follows and the correlation graph are displayed in Fig. 6.

B3LYP level

$$S = 281.84267 + 1.10322T - \left(- 2.40362 \times 10^{-4}T^2 \right) \quad (1)$$

$$\delta H = -10.57948 + 0.11938T + 2.90332 \times 10^{-5}T^2 \quad (2)$$

$$C = 14.89099 + 1.03651T - 4.20155 \times 10^{-4}T^2 \quad (3)$$

HF level

$$S = 288.08499 + 1.03061T - 2.14469 \times 10^{-4}T^2 \quad (4)$$

$$\delta H = -8.02599 + 0.10289\,T + 2.8557 \times 10^{-4}T^2 \quad (5)$$

$$C = 19.9219 + 0.93787\,T - 3.42113 \times 10^{-4}T^2 \quad (6)$$

All of the simulated thermodynamic data are very helpful for further investigations on the thermodynamic parameters of the (2*E*)-IPHC molecule. They can be used to compute the other thermodynamic energies according to the relationships of thermodynamic functions, and estimate directions of chemical reactions according to the second law of.

4.8. Ultraviolet spectra analysis and Frontier molecular orbitals (FMOs)

The highest occupied molecular orbital (HOMO) and the lowest-

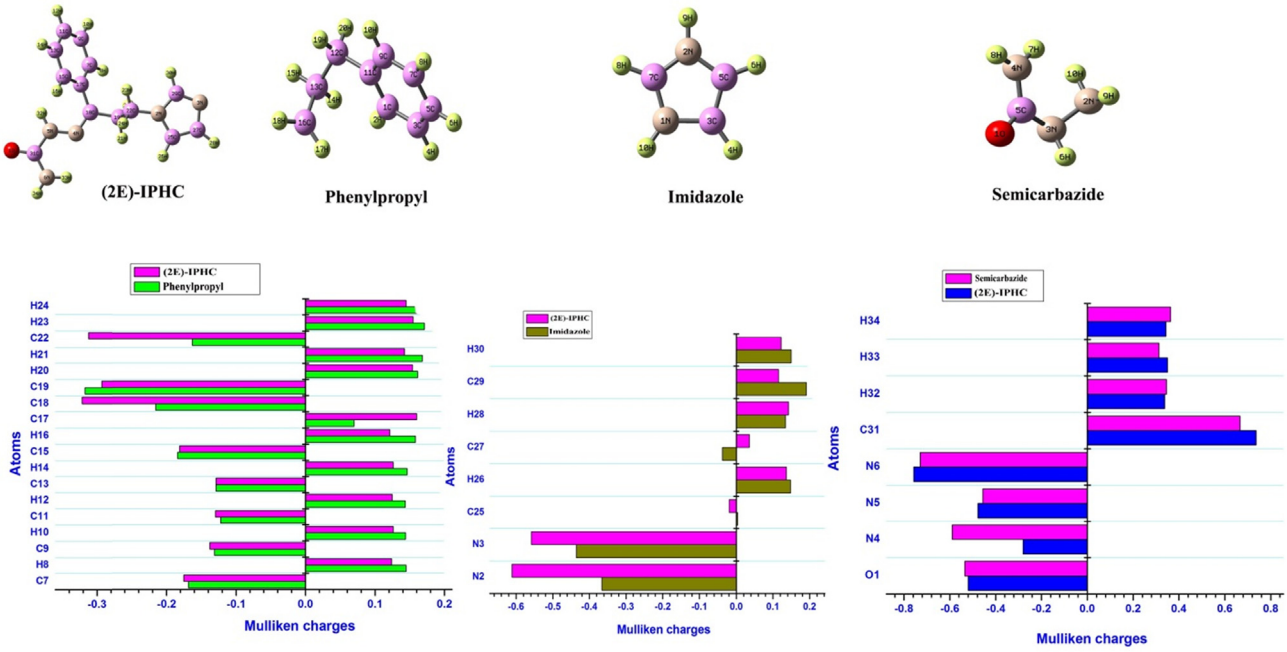

Fig. 4. Comparative Mulliken charge distribution of (2*E*)-IPHC.

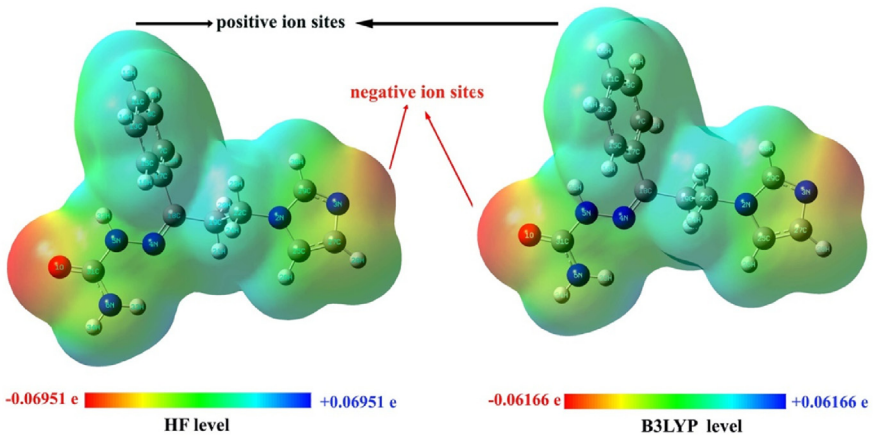

Fig. 5. Molecular electrostatic potential (MEP) map in gas phase of (2*E*)-IPHC.

Table 5
Thermodynamic functions at different temperatures at B3LYP and HF level of (2*E*)-IPHC.

Temperature (K)	S (J/mol.K)		Cp (J/mol.K)		ddH (kJ/mol)	
	B3LYP	HF	B3LYP	HF	B3LYP	HF
100	387.91	385.30	124.51	122.74	8.62	8.51
200	495.49	489.42	197.20	186.85	24.55	23.90
298	589.59	577.57	280.47	260.96	47.96	45.81
300	591.33	579.19	282.06	262.42	48.48	46.29
400	683.91	665.35	363.96	339.47	80.86	76.43
500	772.88	748.68	433.78	408.19	120.86	113.90
600	857.17	828.36	490.46	465.70	167.17	157.69
700	936.33	903.82	536.26	513.05	218.59	206.70
800	1010.47	974.96	573.76	552.22	274.15	260.03
900	1079.90	1041.95	604.94	585.02	333.13	316.94
1000	1145.04	1105.07	631.20	612.79	394.97	376.86

lying unoccupied molecular orbital (LUMO) are named as frontier molecular orbitals (FMOs). The Gauss-Sum 2.2 program [23,24] is used to calculate major and minor energy contributions to the molecular orbitals. The energy gap between HOMO and LUMO determines the kinetic stability, chemical reactivity, optical polarizability, and chemical hardness–softness of the molecule. Chemical hardness and softness can be used as complementary tools in the description of the thermodynamic aspects of chemical reactivity.

Molecular orbital energies are computed in the gas phase, ethanol, DMSO and acetonitrile. The energies of the molecular orbital of the (2*E*)-IPHC molecule are calculated using B3LYP/6-31 + G(d,p) and the values are presented in Table 6. The computed HOMO and LUMO values in the gas phase, ethanol, DMSO, and acetonitrile are −6.1147, −6.1133, −6.1141, −6.1139 and −0.9812, −0.9801, −0.9809, −0.9807 eV, respectively. The energy gap between the HOMO and LUMO was 5.1334 eV in the gas phase and 5.1331 eV in each of the solvents used.

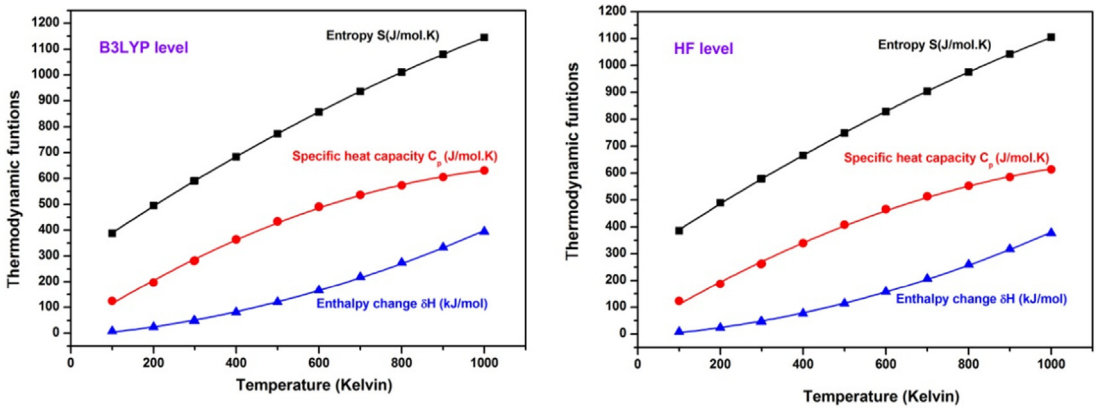

Fig. 6. Correlation graph of thermodynamic functions with temperature of (2*E*)-IPHC.

Table 6
Calculated molecular orbital energies values of (*2E*)-IPHC.

TD-DFT/B3LYP/6-31 + G(d,p)	GAS	Ethanol	DMSO	Acetonitrile
HOMO-1	−6.2340	−6.2283	−6.2321	−6.2307
HOMO	−6.1147	−6.1133	−6.1141	−6.1139
LUMO	−0.9812	−0.9801	−0.9809	−0.9807
LUMO+1	−0.1559	−0.1515	−0.1545	−0.1534
HOMO-LUMO	−5.1334	−5.1331	−5.1331	−5.1331
HOMO-1 − LUMO+1	−6.0781	−6.0767	−6.0775	−6.0773
Electronegativity (χ)	3.5479	3.5467	3.5475	3.5473
Chemical hardness (η)	2.5667	2.5666	2.5666	2.5666
Softness (S)	0.1948	0.1948	0.1948	0.1948
Electrophilicity index (ω)	2.4521	2.4505	2.4516	2.4513
Dipole moment (Debye)	4.7124	4.6419	4.6898	4.6726
SCF Energy (hartrees)	−853.4065	−853.4056	−853.4062	−853.4060

The energy gap between HOMO–LUMO explains the eventual charge transfer interaction within the molecule, which influences its biological activity. 3D plots of the HOMO and LUMO orbitals computed at the B3LYP/6-31 + G(d,p) level in the gas phase for the (2*E*)-IPHC molecule are illustrated in Fig. 7. The orange color represents positive values while the green color represents the negative values. In HOMO and LUMO, the lobes covered the phenyl ring and semicarbazide moiety. The HOMO → LUMO transition implies an electron density transfer.

Electronegativity, chemical hardness, softness, and electrophilicity index of the compound were computed in the gas phase at the B3LYP level and the values are 3.5479, 2.5667, 0.1948, and 2.4521 eV, respectively. The dipole moment and self-consistent field (SCF) energy convergence in the gas phase are 4.7124 Debye and −853.4065 hartrees, respectively. On the other hand, DMSO showed the largest computed dipole moment value (4.6898 Debye) in the liquid phase.

UV analysis of the (2*E*)-IPHC molecule has theoretically been investigated in the gas phase, ethanol, DMSO, and acetonitrile solvents by TD-DFT/B3LYP/6-31 + G(d,p) calculations. Different solvents influence variable binding sites in compounds in distinct ways. The computed values of electronic excitation energies, oscillator strengths and absorption wavelengths are listed in Table 7. The observed and simulated UV graphs are shown in Fig. 8. The computed absorption values were found to be 267.06, 262.05, and 247.83 nm in the gas phase; 267.33, 262.30, and 247.89 nm in ethanol; 267.14, 262.74, and 247.87 nm in DMSO; 267.21, 262.15, and 247.87 nm in acetonitrile. The experimental UV absorption maximum in acetonitrile was observed at 275.52 nm. The major contributions of the transitions were designated with the aid of the SWizard program [25]. In view of the absorption spectra, the maximum absorption wavelength corresponds to the electronic transition from HOMO-1 to LUMO with 65% contribution. The other wavelength, excitation energies, oscillator strength and calculated counterparts with major contributions can be seen in Table 7.

4.9. Vibrational analysis

The observed vibrations are active with different shapes and intensities in Raman and infrared. The title molecule has 34 atoms and with assumed C_s point group symmetry. The vibrational modes were computed at the B3LYP level in the gas phase and were compared with the experimental values and the calculated potential energy distributions (PED) as shown in Table 8. The assignments of the observed wavenumbers from FT-IR and FT-Raman spectra were based on the normal mode analyses. The observed and simulated FT-IR and FT-Raman spectra of the (2*E*)-IPHC molecule are shown in Figs. 9 and 10, respectively.

4.9.1. Amide group vibrations

The amide group vibrations normally appear in the regions of 3550–3330 cm^{-1} and at 3450–3250 cm^{-1} for asymmetric and symmetric stretching, respectively [26]. In the molecule under study, there are three expected NH vibrations in the semicarbazide moiety. At this same position, in the FT-IR, two NH asymmetric stretching vibrations were observed at 3463 and 3440 cm^{-1}. The single NH vibration was computed as 3392 cm^{-1} and it was assigned as symmetric stretching. The observed and computed values are within the expected range. The NH_2 scissoring vibrations were found in the range of 3550–3330 cm^{-1}. This mode of vibration was observed with high intensity in the FT-Raman at 1560 cm^{-1} and the computed value was calculated

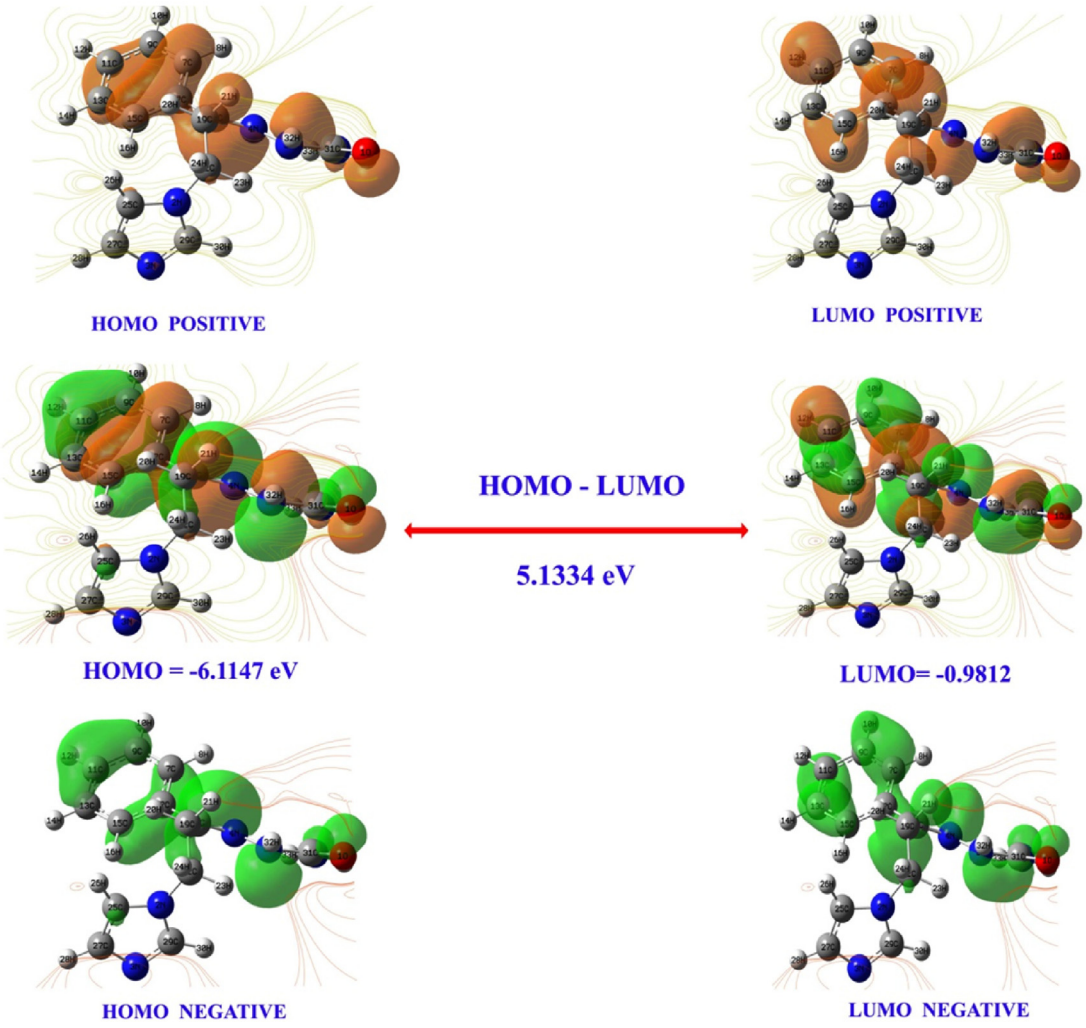

Fig. 7. Molecular orbitals and energies for the HOMO and LUMO of (2*E*)-IPHC in the gas phase.

Table 7
Computed excitation energies E (eV), absorption wavelength λ (nm), and oscillator strengths (*f*) using TD-DFT/B3LYP/6-31 + G(d,p) method for (2*E*)-IPHC.

Medium	Energy (eV)	Wavelength (nm)	Oscillator strength	Major contribution of energy
GAS	4.6425	267.06	0.0006	HOMO-1- > LUMO (99%)
	4.7312	262.05	0.5451	HOMO- > LUMO (96%)
	5.0026	247.83	0.0009	HOMO-2- > LUMO (55%)
Ethanol	4.6378	267.33	0.0006	HOMO-1- > LUMO (99%)
	4.7267	262.30	0.5507	HOMO- > LUMO (96%)
	5.0014	247.89	0.0009	HOMO-2- > LUMO (55%),
DMSO	4.6410	267.14	0.0006	HOMO-1- > LUMO (99%)
	4.7188	262.74	0.5624	HOMO- > LUMO (96%)
	5.0019	247.87	0.0009	HOMO-2- > LUMO (55%)
Acetonitrile	4.6399	267.21	0.0006	HOMO-1- > LUMO (99%)
	4.7294	262.15	0.5473	HOMO- > LUMO (96%)
	5.0019	247.87	0.0009	HOMO-2- > LUMO (55%)

as 1558 cm^{-1}. The PED was calculated as a mixed mode with in-plane bending C—H and its individual contribution was computed as 72%. The single N—H in-plane bending was computed as 1413 cm^{-1}. One rocking NH_2 vibration appeared at 1098 cm^{-1} with weak intensity in the FT-Raman spectrum. The out-of-bending N—H modes were shown in the expected range. Most of the in-plane and out-of-plane bending vibrations were computed with PED less than 50%.

4.9.2. C—H vibrations

In the title compound, the C—H vibrations are due to the phenylpropyl and imidazole moieties. Aromatic compounds commonly exhibit multiple weak bands in the region of 3100—3000 cm^{-1} due to aromatic C—H stretching vibrations. They are not appreciably

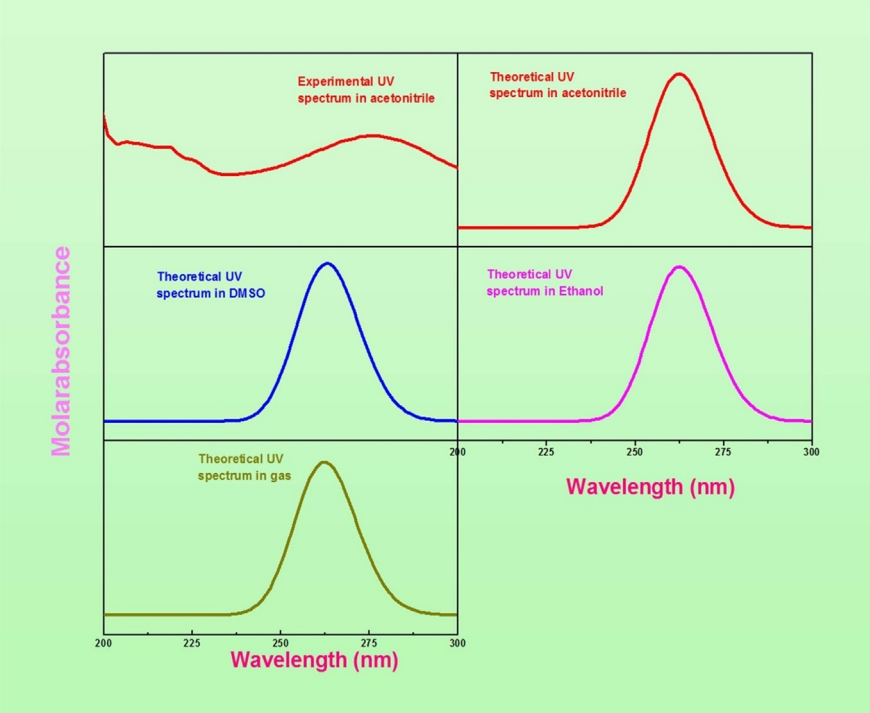

Fig. 8. Experimental and simulated UV spectra of (2*E*)-IPHC.

affected by the nature of the substituents [27]. Four aromatic, three imidazole, and four methylene C–H vibrations were expected in the (2*E*)-IPHC molecule. The FT-IR band at 3150 cm^{-1} and FT-Raman bands at 3130, 3125, 3076, and 3066 cm^{-1} were observed and assigned as ring C–H stretching. Three vibrations were observed at 2990, 2951, and 2938 cm^{-1} and were assigned to the methylene groups in the (2*E*)-IPHC molecule. Their computed values were at 3007, 2988, 2952, and 2934 cm^{-1} with average PED of about 90%. The bands were observed with very weak intensities. The in-plane bending modes of the phenyl ring of the (2*E*)-IPHC molecule appeared at 1482, 1460, 1444, and 1434 cm^{-1} and out-of-plane bending at 933, 906, and 830 cm^{-1}. The PED values are in the range of 61–97%.

The computed values of the imidazole ring in-plane bending modes of the title compound are presented at 1373, 1354, and 1262 cm^{-1} and out-of-plane bending at 770, 776, and 688 cm^{-1}. The CH_2 scissoring vibrations were computed as 1373 and 1354 cm^{-1}. A vibration was observed in the FT-IR at 1342 cm^{-1} with strong intensity and was assigned as CH_2 scissoring. A NH_2 rocking vibration was calculated at 1274 and 1269 cm^{-1} and the observed band was found at 1275 cm^{-1} in FT-Raman. The CH_2 twisting and wagging were found in the anticipated range.

4.9.3. C=O vibrations

The C=O stretching and the NH_2 scissoring deformation vibrations overlap each other in the hydrogen-bonded state. The C=O stretch is the stronger band in the infrared and absorbs usually in the range of 1680–1640 cm^{-1}. Similarly, C=O stretching overlapped with N–H, and N–H stretching appeared around 3300 cm^{-1} [28]. In the FT-IR spectrum of (2*E*)-IPHC, a very strong band was found at 1690 cm^{-1} and was assigned to the C=O stretching type of vibration. The N–C=O in-plane bending deformation normally appears at 600–550 cm^{-1}. In the present investigation, it appeared at 538 cm^{-1} in FT-Raman with medium intensity. The calculated value is presented at 534 cm^{-1} with PED value 46%.

4.9.4. C–C vibrations

Aromatic C=C stretching modes occur in the region of 1620–1400 cm^{-1} and it is called ring mode. C=C and C=O bonds interact strongly in the same region because the masses of carbon and oxygen atoms do not differ greatly. The bands in the range of 1650–1400 cm^{-1} were assigned to the C=C stretching mode [29,30]. The C=C stretching vibrations were found at 1590, 1576, and 1501 cm^{-1} and the C–C stretching vibrations were observed at 1285, 1247, and 1145 cm^{-1}. All bands appeared with strong and medium intensities in both FT-IR and FT-Raman. The computed values fit well with the observed values and appeared in the expected range. The imidazole ring C–C stretching vibration was observed at 1019 cm^{-1} with weak intensity in the FT-Raman spectrum. The PED values for C=C bonds are 60–64% and for C–C bonds are 30–35%. The aromatic in-plane CCC bending vibrations were obtained at 970 and 705 cm^{-1} in the FT-IR spectrum, while the CCC out-of-plane bending vibrations were observed at 675 and 585 cm^{-1} in the FT-Raman and FT-IR spectra of the (2*E*)-IPHC molecule. The vibrations were observed with strong and medium intensities which is reflected in the PED around the range of 24–58%.

4.9.5. C=N, C–N and N=N vibrations

Compounds containing a C=N group are characterized by the C=N stretching band in the FT-IR and FT-Raman spectra. However, the C=N stretching frequency is expected to be phase-sensitive, since the C=N moiety is a polar functionality. The C–N stretching absorptions appear in the region of 1382–1266 cm^{-1} for aromatic amines [31,32]. The infrared band of the C=N stretching mode is often found between those of the C=O and C=C stretching modes. Medium intensity bands were observed at 1602 and 1613 cm^{-1} in the FT-IR and FT-Raman spectra, respectively, of the title molecule and they were assigned as the C=N stretching vibrations. The in-plane bending of the C=N vibration was observed at 630 cm^{-1} in the FT-IR spectrum of the (2*E*)-IPHC molecule.

Table 8
Detailed assignments of theoretical wavenumbers of (*2E*)-IPHC.

Experimental wavenumbers[a]		B3LYP/6-31G(d,p) wavenumbers				Mode description[b]
FT-IR	FT-Raman	Unscaled	Scaled	I_{IR}	S_{Raman}	
3463 vw		3724	3575	2.15	1.67	γNH(98)
3440 m		3594	3451	2.26	2.12	γNH(98)
3395 vw		3533	3392	0.07	9.37	γNH(100)
3150 m		3286	3155	0.42	2.34	γCH(99)
3130 vw	3130 vw	3259	3129	0.70	1.62	γCH(97)
	3125 vw	3255	3125	1.13	5.09	γCH(96)
		3217	3088	4.27	2.51	γCH(90)
	3076 vw	3208	3079	1.05	2.19	γCH(94)
		3201	3073	0.59	1.44	γCH(90)
	3066 vw	3193	3065	1.81	5.21	γCH(93)
		3188	3060	1.18	1.11	γCH(92)
		3133	3007	8.87	4.09	γCH(91)
	2990 vw	3113	2988	3.03	2.55	γCH(87)
2951 w		3075	2952	1.25	2.27	γCH(87)
	2938 vw	3057	2934	13.53	0.75	γCH(94)
1690 s		1833	1760	126.80	3.58	γC = O(73)
1602 m	1613 m	1681	1614	97.77	5.19	γC = N(77)
	1590 vs	1659	1592	6.69	2.15	γCC(63) + βCH(19)
1576 s		1633	1568	7.06	0.61	γCC(65) + βCH(11)
	1560 s	1623	1558	23.18	2.24	βNH(72) + βCH(10)
	1501 s	1559	1496	43.87	3.53	γCC(62) + βCH(17)
		1547	1485	47.77	1.71	γCC(24) + βCH(65)
	1482 vw	1542	1480	43.24	5.13	γCC(56) + βCH(16)
	1460 vw	1520	1459	4.71	9.01	βCH(67)
1444 s		1503	1443	9.67	4.21	βCH(61)
	1434 vw	1493	1433	5.66	3.51	βCH(68) + γCC(28)
		1471	1413	30.53	1.21	βCH(44) + γCN(16)
		1430	1373	5.20	4.69	βCH(38) + γCC(20)
	1360 vw	1419	1362	15.65	0.15	γCN(34)
1342 m		1410	1354	28.56	1.16	ϕC = N(50)
1330 vw		1401	1345	16.34	1.49	γCN(53)
1319 m		1370	1315	8.56	1.03	βCH(70) + γCC(14)
1285 m		1339	1285	21.99	1.65	βCH(61) + γCC(10)
	1275 m	1327	1274	11.20	3.28	βCH(46)
		1322	1269	22.89	1.09	βCH(25)+βCN(11
		1314	1262	11.52	0.89	βCH(27) + γCC(12)
1247 m		1295	1243	12.28	3.33	γCC(34)
1228 m		1271	1220	2.53	1.16	βCN(57) + γCN(11)
1170 m		1218	1169	0.57	6.77	βCH(76) + γCC(11)
		1197	1149	12.72	3.20	βCH(81) + γCC(13)
1145 m		1195	1147	2.49	2.19	βCH(32) + γNN(14)
	1128 vw	1173	1126	0.54	1.05	γNN(41)
1104 m		1151	1104	3.58	5.84	γCN(44) + βCH(28)
	1098 vw	1142	1096	0.23	0.17	βNH(34) + γCC(13)
1069 m		1112	1067	3.44	29.66	γCC(40) + βCH(32)
	1062 vw	1104	1060	7.69	30.11	βCH(47) + γCC(14)
	1049 w	1096	1052	5.70	7.64	γCC(20) + βCN(15)
	1019 w	1056	1014	39.68	1.41	γCC(37) + βCCC(23)
	1008 m	1051	1009	4.80	18.96	βCN(19) + γCN(16)
		1039	997	28.96	5.15	γCN(20)+βCN(10)
		1028	987	35.47	10.23	γCC(61)
970 w		1017	976	20.53	1.05	ϕCCC(56) + γCC(25)
		1005	964	9.88	12.55	ϕCH(77) + ϕCCC(14)
		981	942	13.71	6.98	γCN(73)
933 m		978	938	68.84	8.10	ϕCH(82) + ϕCCC(11)
906 m		942	904	76.52	22.45	ϕCH(89)
		915	879	0.06	5.38	βCCN(79)
830 w		868	833	1.33	5.46	ϕCH(97)
		851	817	37.51	8.50	ϕHCN(80)
		817	784	54.59	27.17	ϕCH(24) + βCCN(10)
		802	770	49.52	18.14	ϕHCN(66)
765 s		801	767	20.00	36.10	ϕCH(42)
		758	728	12.26	5.87	ϕCH(36)
		751	720	17.98	10.51	ϕCON(55)
705 m		743	714	3.49	1.51	ϕCON(35)
		717	688	5.07	18.14	ϕCH(80
	675 m	717	688	13.73	59.19	ϕCCC(44) + ϕCH(33)
	640 m	676	649	233.16	6.71	ϕCCC(76) + ϕCH(10)
630 m		654	628	1.52	12.52	ϕNCC(21)
		652	626	200.07	2.07	βCCN(58) + ϕCCNC(13)
		633	607	36.47	5.10	βCCC(58) + ϕCCNC(23)
		625	600	51.91	21.42	ϕCCNC(33) + βCCC(19)

(*continued on next page*)

Table 8 (*continued*)

Experimental wavenumbers[a]		B3LYP/6-31G(d,p) wavenumbers				Mode description[b]
FT-IR	FT-Raman	Unscaled	Scaled	I_{IR}	S_{Raman}	
585 w		614	589	14.23	1.98	ϕCCN(48)
		580	557	3.87	2.75	ϕHNNC(66) + ϕHNCN(12)
	538 m	556	534	42.22	7.05	βNCO(46) + ϕHNCN(14)
489 m		501	481	29.12	2.24	ϕHNCN(53) + βNCO(13)
		485	466	325.28	20.11	βCCN(31)
	441 vw	461	443	2.42	17.89	ϕCCCC(41) + βCCN(12)
398 vw		412	395	0.90	109.60	ϕCCCC(68) + ϕHCCC(17)
		393	378	29.42	334.79	ϕCCNN(58)
		370	356	471.74	34.25	ϕHNCN(60)
	342 vw	356	342	5.25	95.88	βCCN(46) + ϕHNCN(10)
		310	298	29.63	25.18	βCNCN(31)
		295	283	0.85	79.54	βCCCN(28)
	243 vw	254	244	20.20	3.41	βCCCN(31)
	215 vw	215	207	2.47	14.24	βCCCC(44)
	165 vw	181	174	0.15	95.96	ϕCCNN(49)
	121 m	133	128	9.01	88.40	βCCCC(25) + ϕCCNC(13)
	93 w	93	89	23.14	26.79	ϕCCNC(34)
		70	67	15.29	304.89	ϕNCNN(46)
		69	66	4.95	38.63	ϕCCCC(45)
		62	60	6.05	118.46	ϕCCCN(51)
		47	45	3.66	90.49	ϕCCCC(48)
		40	38	17.76	110.02	ϕCCCC(67)
		28	26	28.44	140.52	ϕCCCC(53)
		25	24	76.73	68.36	ϕCCCN(27)

[a] s: strong; vs: very strong; m: medium; w: weak; vw: very weak.
[b] ν: stretching; β: in-plane bending; γ: out-of-plane bending; I_{IR}: IR intensity, S_{Raman}: Raman scattering activity.

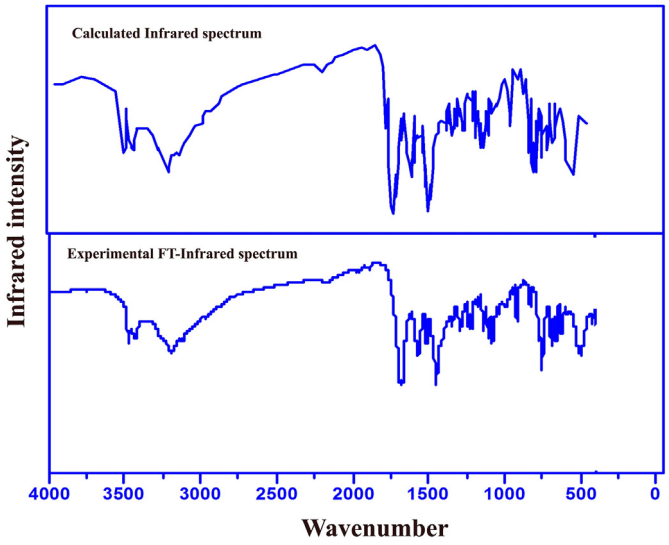

Fig. 9. Experimental and simulated Infrared spectra of (2*E*)-IPHC.

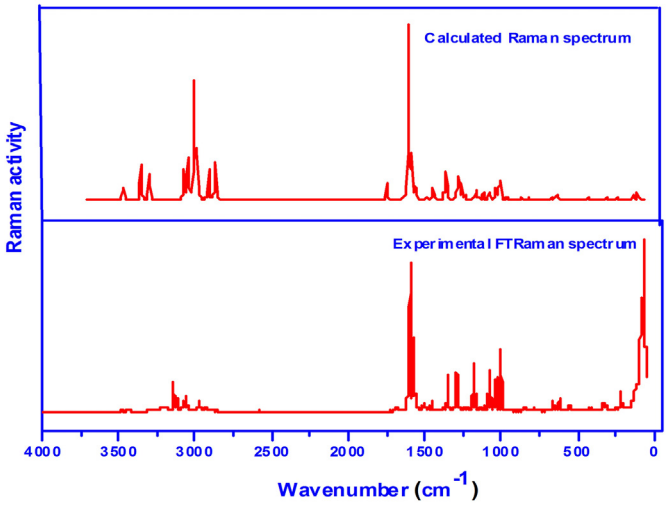

Fig. 10. Experimental and simulated Raman spectra of (2*E*)-IPHC.

The C—N stretching vibrations are usually mixed with other vibrations and are difficult to identify in the spectrum. Seven C—N stretching modes are expected to be observed in the (2*E*)-IPHC molecule. Three stretching modes were identified at 1330, 1104, and 1008 cm^{-1} (imidazole) in addition to one C—N stretching mode at 1360 cm^{-1} (semicarbazide) with a very weak intensity in the FT-Raman spectrum of the (2*E*)-IPHC molecule. The in-plane and out-of-plane bending modes of C—N vibrations were found in the expected range.

N—N stretching vibration appeared at 1128 cm^{-1} with a very weak intensity in the FT-Raman spectrum of the (2*E*)-IPHC molecule. While, the computed FT-Raman in-plane and out-of-plane bending were found at 770 and 67 cm^{-1} with PED values of 66 and 46%, respectively.

4.10. NMR analysis

Nuclear magnetic resonance (NMR) is an important analytical tool to elucidate the chemical structure of organic compounds. The experimental NMR (^{1}H and ^{13}C) spectra were analyzed and fit to the correct values with the aid of computed calculations. The experimental and simulated proton and carbon NMR of (2*E*)-IPHC are shown in Fig. 11. The observed and computed NMR (2*E*)-IPHC chemical shifts are given in Table 9. The NMR chemical shifts were computed in DMSO and acetonitrile solvents and were compared with observed values. In the ^{13}C NMR spectrum, the signal at 145.1 ppm was assigned to be due to C31 bonding with the oxygen (O1) atom. Similarly, the peak at 153.6 ppm was assigned to the C18 double bond to the nitrogen atom. The ^{13}C NMR of the phenyl ring in the (2*E*)-IPHC molecule was observed between 128.4 and

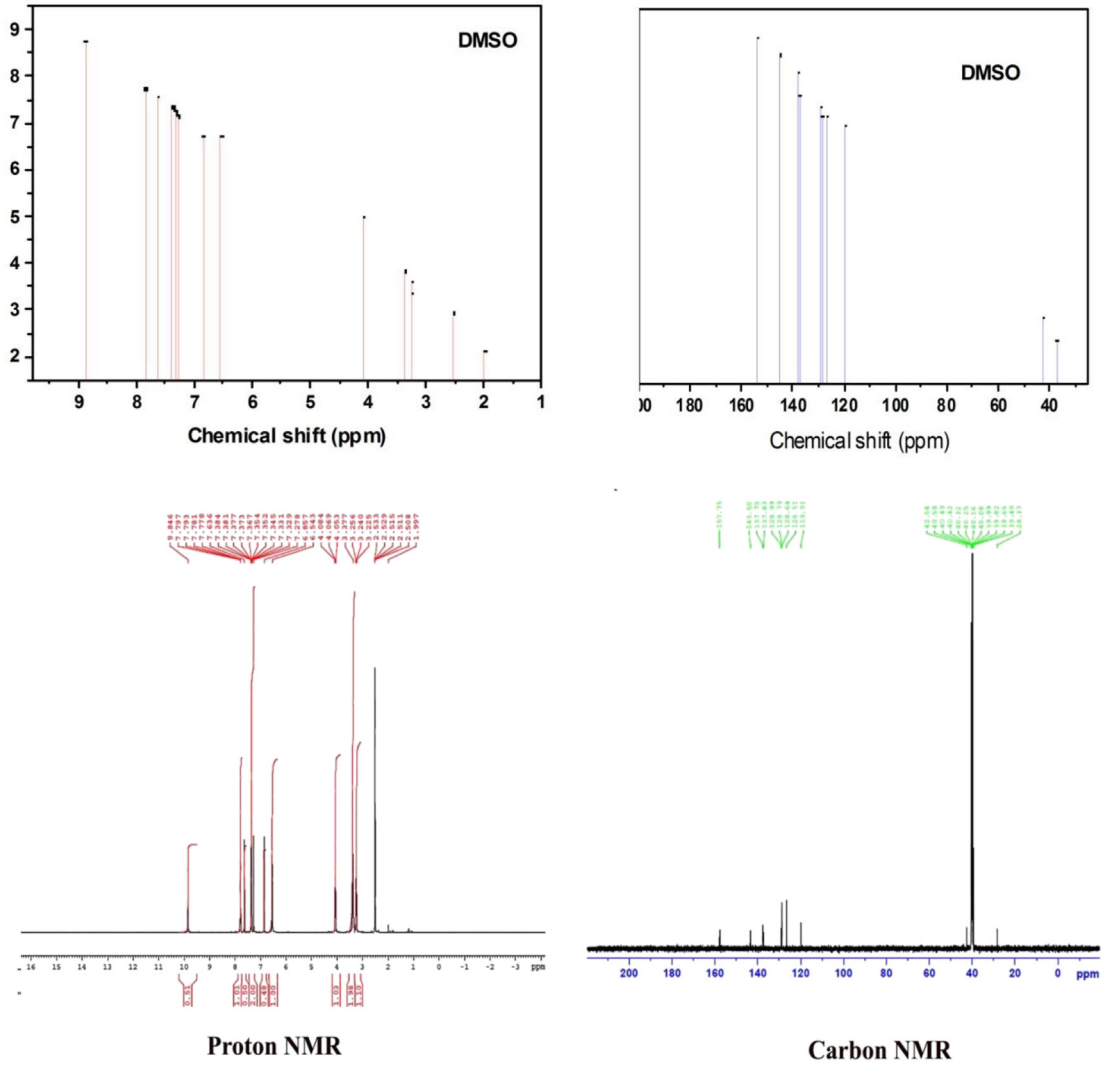

Fig. 11. The simulated (upper) and experimental (lower) proton and carbon NMR spectra of (2*E*)-IPHC.

Table 9
Experimental, calculated (corrected) ^{13}C and ^{1}H NMR isotropic chemical shifts (ppm) of (*2E*)-IPHC.

^{13}C				^{1}H			
Atom	δ_{exp}	δ_{cal} (B3LYP)		Atom	δ_{exp}	δ_{cal} (B3LYP)	
		DMSO	Acetonitrile			DMSO	Acetonitrile
C7	129.4	125.1	125.1	H8	7.85	7.58	7.57
C9	128.4	127.2	127.2	H10	7.34	7.36	7.36
C11	128.5	127.2	127.2	H12	7.06	7.15	7.15
C13	128.4	123.9	123.9	H14	7.34	7.20	7.20
C15	129.4	135.9	135.9	H16	7.85	7.75	7.74
C17	136.8	145.1	145.1	H20	3.34	2.95	2.95
C18	153.6	159.2	159.2	H21	3.34	2.13	2.13
C19	28.3	37.4	37.4	H23	4.13	3.61	3.60
C22	42.1	47.0	47.0	H24	4.13	3.36	3.35
C25	119.4	114.9	114.9	H26	6.87	6.72	6.72
C27	119.9	127.3	127.4	H28	7.29	6.74	6.74
C29	137.3	131.4	131.4	H30	7.65	7.29	7.29
C31	145.1	151.9	151.8	H32	8.89	8.75	8.74
				H33	7.40	4.99	4.99
				H34	7.40	3.84	3.83

136.8 ppm. The chemical shifts of the imidazole ring carbons were also found in the range of 119.4–137.3 ppm. The chemical shifts of methylene carbon atoms C19 and C22 were predicated with the lowest carbon chemical shifts of 37.4 and 47.0 ppm, respectively.

In the ^{1}H NMR spectrum of (2*E*)-IPHC, eleven peaks were observed between 3.34 and 8.89 ppm. The proton NMR chemical shift signal splitting is caused by spin-spin coupling between nearest nuclei. The ^{1}H NMR signals of methylene protons in the side chain were observed at 3.34 and 4.13 ppm, which were assigned to be due to the equivalent protons H20, H21 and H23 and H24 atoms, respectively. The phenyl ring protons appeared in the range of 7.06–7.85 ppm. A similar trend was observed in the imidazole ring protons, the ^{1}H NMR of H26 appeared at 6.87 ppm and the remaining H28 and H30 atoms appeared at 7.29 and 7.65 ppm, respectively.

The correlations between the experimental and computed chemical shifts were obtained by the B3LYP method in DMSO and acetonitrile. The relations between the computed and experimental carbon and hydrogen chemical shifts are linear and described by the following equations:

^{13}C NMR

$$\delta_{cal}(ppm) = 1.06487\ \delta_{exp} + 1.0123\left(R^2 = 0.9920\right) in\ DMSO \quad (7)$$

$$\delta_{cal}(ppm) = 1.07725\ \delta_{exp} + 1.0122\left(R^2 = 0.9921\right) in\ acetonitrile \quad (8)$$

^{1}H NMR

$$\delta_{cal}(ppm) = -0.44728\ \delta_{exp} + 1.1627\left(R^2 = 0.8588\right) in\ DMSO \quad (9)$$

$$\delta_{cal}(ppm) = -0.45375\ \delta_{exp} + 1.1633\left(R^2 = 0.8590\right) in\ acetonitrile \quad (10)$$

The calculated chemical shift values for both ^{1}H and ^{13}C NMR showed good linear fitting with the experimental values according to the regression values (0.86–0.99).

5. Conclusions

The potential energy scan of the anticonvulsant agent named (2*E*)-2-[3-(1*H*-imidazol-1-yl)-1-phenylpropylidene]hydrazine-carboxamide ((2*E*)-IPHC) was used to identify the most stable conformer with the global minimum energy. The investigations of the optimized molecular geometry showed that there was a considerable change in the bond lengths (CH, CC, CN, and CO) and bond angles (CCC, CCN, HNN, NCC, and HNC) between the phenylpropyl, semicarbazide, and imidazole moieties of the (2*E*)-IPHC molecule but they deviate less from the experimental values. In the AIM analysis, the interaction energy and total electron density variation, charge density range and Laplacian charge density range were analyzed. All hydrogen atoms in the (2*E*)-IPHC molecule exhibited positive values and there was not much deviation in charge distribution. Mulliken charges in the carbonyl and amide groups could contribute positively to the displayed biological activity of the title molecule. In view of the calculated absorption spectra, the maximum absorption wavelength corresponds to the electronic transition from HOMO-1 to LUMO with a 65% contribution. Most of the amino group in-plane and out-of-plane bending vibrations were computed with PED less than 50%. The twisting and wagging of the methylene group were found in the anticipated range. The infrared band of the C=N stretching mode was found between those of the C=O and C=C stretching modes. The computed values for both ^{1}H and ^{13}C NMR showed good linear fitting with the experimental values as evidenced by the regression values around 0.90.

Acknowledgments

The authors would like to extend their sincere appreciation to the Deanship of Scientific Research at King Saud University for its funding of this research through the Research Group Project No. RGP-VPP-196.

References

[1] W. Loscher, Eur. J. Pharmacol. 342 (1998) 1–13.
[2] A. Husain, M.A. Naseer, M. Sarafroz, Acta Pol. Pharm. Drug Res. 66 (2009) 135–140.
[3] S. Malik, R.S. Bahare, S.A. Khan, Eur. J. Med. Chem. 67 (2013) 1–13.
[4] L.A. Clutterbuck, C.G. Posada, C. Visintin, D.R. Riddall, B. Lancaster, P.J. Gane, J. Garthwaite, D.L. Selwood, J. Med. Chem. 52 (2009) 2694–2707.
[5] L. Blanch, J. Galvez, R. Domenech, Bioorg. Med. Chem. 13 (2003) 2749–2754.
[6] K.K. Madsen, R.P. Clausen, O.M. Larsson, P. Krogsgaard-Larsen, A. Schousboe, H.S. White, J. Neurochem. 109 (2009) 139–144.
[7] A. Thiry, J.M. Dogne, C.T. Supuran, B. Masereel, Curr. Top. Med. Chem. 7 (2007) 855–864.
[8] P.E. Penovich, L.J. Willmore, Epilepsia 50 (2009) 37–41.
[9] J. Rémi, A. Hüttenbrenner, B. Feddersen, S. Noachtar, Epilepsy Res. 88 (2010) 145–150.
[10] M.I. Attia, M.N. Aboul-Enein, A.A. El-Azzouny, Y.A. Maklad, H.A. Ghabbour, Sci. World J. 2014 (2014) 1–9.
[11] K.B. Benzon, H.T. Varghese, C.Y. Panicker, K. Pradhan, B.K. Tiwary, A.K. Nanda, C. Van Alsenoy, Spectrochim. Acta A 151 (2015) 965–979.
[12] N. Sundaraganesan, S. Ilakiamani, P. Subramani, B.D. Joshua, Spectrochim. Acta A 67 (2007) 628–635.
[13] K.B. Benzon, H.T. Varghese, C.Y. Panicker, K. Pradhan, B.K. Tiwary, A.K. Nanda, C. Van Alsenoy, Spectrochim. Acta A 146 (2015) 307–322.
[14] A. Frisch, A.B. Nielsen, A.J. Holder, Gaussian Inc., Pittsburg, PA, 2000.
[15] F. Sen, M. Dinçer, A. Cukurovali, Spectrochim. Acta A 150 (2015) 257–267.
[16] R.I. Dennington, T. Keith, J. Millam, K. Eppinnett, W.L. Hovell, R. Gilliland, Gauss View Version 3.09, Semichem. Inc., Shawnee Mission, KS, 2003.
[17] M.H. Jamróz, Vibrational Energy Distribution Analysis, VEDA 4, Warsaw, 2004.
[18] M.I. Attia, H.A. Ghabbour, H.-K. Fun, Z. Kristallogr. NCS 230 (2015) 249–250.
[19] R.F.W. Bader, Atoms in Molecules, a Quantum Theory, Oxford University Press, Oxford, 1990.
[20] F.W. Biegler-Köning, J. Schönbohm, D. Bayles, J. Comput. Chem. 22 (2001) 545–559.
[21] U. Koch, P.L.A. Popelier, J. Phys. Chem. 99 (1995) 9747–9754.
[22] J.B. Ott, J. Boerio-Goates, Calculations from Statistical Thermodynamics, Academic Press, 2000.
[23] I. Fleming, Frontier Orbitals and Organic Chemical Reactions, Wiley, London, 1976.
[24] N.M. O'Boyle, A.L. Tenderholt, K.M. Langner, J. Comput. Chem. 29 (2008) 839–845.
[25] S.I. Gorelsky, SWizard Program Revision 4.5, University of Ottawa, Ottawa, Canada, 2010.
[26] S.J. Simgh, S.M. Pandey, Indian J. Pure Appl. Phys. 12 (1974) 300–302.
[27] G. Varsanyi, Vibrational Spectra of Benzene Derivatives, Academic Press, New York, 1969.
[28] F.R. Dollish, W.G. Fateley, F.F. Bentley, Characteristic Raman Frequencies of Organic Compounds, John Wiley & Sons, New York, 1974.
[29] A. Altun, K. Gölcük, M. Kumru, J. Mol. Struct. THEOCHEM 625 (2003) 17–24.
[30] V. Krishnakumar, R.J. Xavier, Indian J. Pure Appl. Phys. 41 (2003) 95–98.
[31] G. Shakilaa, S. Periandy, S. Ramalingam, Spectrochim. Acta A 78 (2011) 732–739.
[32] T. Sivaranjini, S. Periandy, M. Govindarajan, M. Karabacak, A.M. Asiri, J. Mol. Struct. THEOCHEM 1056 (2014) 176–188.